Chemistry & Biology, Vol. 10, 663–672, July, 2003, ©2003 Elsevier Science Ltd. All rights reserved. DOI 10.1016/S1074-5521(03)00147-9

Preferred RNA Binding Sites for a Threading Intercalator Revealed by In Vitro Evolution

Coby B. Carlson, Momchilo Vuyisich, Barry D. Gooch, and Peter A. Beal*
Department of Chemistry
University of Utah
Salt Lake City, Utah 84112

Summary

In pursuit of small molecules capable of controlling the function of RNA targets, we have explored the RNA binding properties of peptide-acridine conjugates (PACs). In vitro evolution (SELEX) was used to isolate RNAs capable of binding the PAC Ser-Val-Acr-Arg, where Acr is an acridine amino acid. The PAC binds RNA aptamers selectively and with a high degree of discrimination over DNA. PAC binding sites contain the base-paired 5′-CpG-3′ sequence, a known acridine intercalation site. However, RNA structure flanking this sequence causes binding affinities to vary over 30-fold. The preferred site (K_D = 20 nM) contains a base-paired 5′-CpG-3′ step flanked on the 5′ side by a 4 nt internal loop and the 3′ side by a bulged U. Several viral 5′- and 3′-UTR RNA sequences that likely form binding sites for this PAC are identified.

Introduction

The development of low molecular weight compounds that bind RNA selectively is a research topic receiving increasing attention [1–5]. One reason for this interest is the appreciation of RNA as a viable target for new antibiotic drugs. There are several examples of clinically useful compounds that bind to RNA of a pathogenic organism [6]. For instance, the macrolide antibiotic erythromycin A binds to the 23S ribosomal RNA of bacteria near the peptidyl transferase loop, inhibiting the translocation step in protein synthesis [7]. Compounds that bind other functionally important RNAs unique to a pathogen could be developed into new therapeutics.

Small molecules that bind RNA can also lead to the control of the activity of individual proteins. This has been demonstrated through regulation of translation of a particular protein by a small molecule binding to its mRNA and via the use of ligand-regulated RNA aptamers that function as tunable inhibitors of a protein's activity [8, 9]. Thus, in addition to their potential as new antibiotics, small molecules that bind RNA selectively are useful tools for chemical biology.

Unfortunately, our lack of understanding of the recognition of RNA by low molecular weight compounds limits our ability to design new, high-affinity ligands for different RNA targets. Consequently, the systematic discovery of RNA-specific compounds is a field still in its infancy [3, 10, 11]. Interestingly, potential RNA targets typically have regions of duplex secondary structure to which numerous compounds, including ethidium, acridine, and ellipticine, bind via intercalation [12]. These compounds, however, do not bind the RNA with a high degree of selectivity and show little or no preference for binding RNA over DNA in general. In spite of this, a potential strategy for rendering an intercalator RNA selective has been suggested [13]. Since the rates of base-pair opening in structured RNA vary with proximity to duplex irregularities (e.g., internal loops) [14], one might target these sites with a threading intercalator.

Threading intercalation involves insertion of an intercalator between base pairs of a nucleic acid duplex and localization of distinguishable substituents on the heterocycle in opposite grooves of the helix [15–17]. One of the side chains is required to pass through the duplex (or thread) during the binding event, thus giving this binding mode its name. Since a transient opening of the double helix at the binding site is necessary, these molecules may bind preferentially to dynamic base-paired locations in an RNA target. In addition, the major and minor grooves of duplex RNA contain functional groups that provide unique recognition surfaces. Indeed, proteins that bind duplex RNA specifically (the dsRBM family of proteins) achieve their specificity by making multiple contacts to 2′-hydroxyls and other groups present in the RNA minor groove [18]. Thus, we have focused our efforts to develop RNA-selective small molecules on compounds that have the potential to bind via threading intercalation.

To this end, we have reported solid-phase synthesis protocols [19, 20] and screening strategies [21] for libraries of substituted acridine derivatives. The acridine core of these compounds is modified with variable peptide substituents emanating from the 4- and 9-positions (Figure 1A), the substitution pattern of a known threading intercalator [22]. We have termed our version of this structure the peptide-acridine conjugate, or PAC. The inspiration for the design of these molecules comes from nucleic acid binding natural products, such as nogalamycin, which is a DNA sequence-selective threading intercalator (Figure 1B). Nogalamycin binds with its anthraquinone intercalated and its nogalose and aminopyranose substituents in the minor and major grooves of duplex DNA, respectively [15, 23]. Its preferred binding sites are 5′-PypG-3′ steps within A•T-rich tracts [24]. This has been rationalized by the observation in X-ray crystal structures of groove contacts between the carbohydrate substituents and G•C base pairs, and the fact that A•T-rich DNA has a higher rate of base pair opening than G•C-rich or mixed sequence DNA [15, 24].

Since threading intercalators may bind selectively to duplex sites in RNA with unusual characteristics, such as non-Watson-Crick flanking structure or short base pair lifetimes, we carried out in vitro evolution (SELEX) experiments designed to identify RNA motifs predisposed to bind to a particular PAC. The highest-affinity RNA binding sites for the PAC studied consist of base-paired 5′-CpG-3′ steps flanked on the 5′ side by an internal loop and on the 3′ side by a U bulge. These

*Correspondence: beal@chemistry.utah.edu

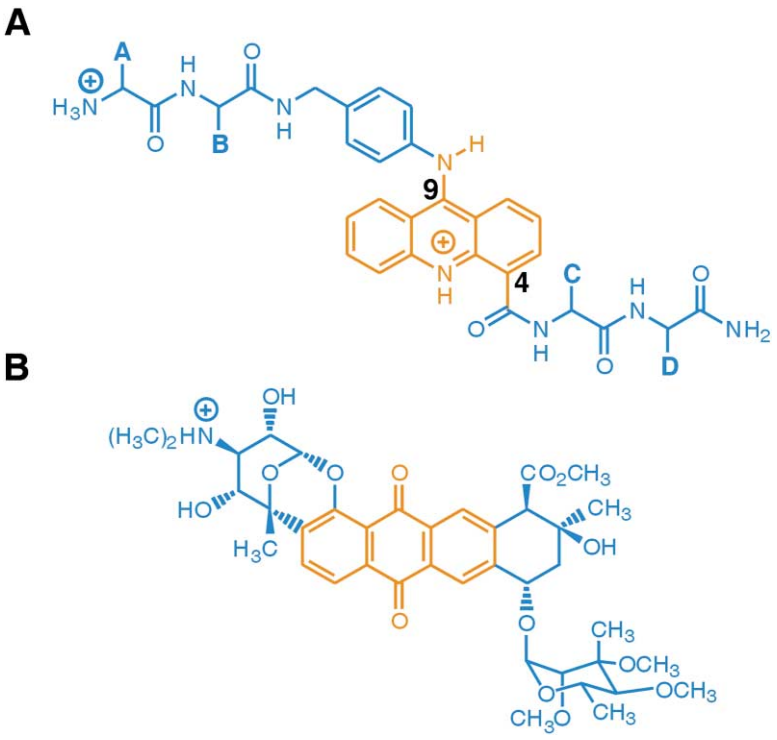

Figure 1. Chemical Structures of Small Molecules that Bind Nucleic Acids by Threading Intercalation

(A) Design of a peptide-acridine conjugate (PAC).

(B) The natural product, nogalamycin. The intercalating group in each structure is highlighted in orange.

results provide the basis for the design of PAC libraries to target this motif in naturally occurring, functionally important RNA molecules.

Results

Selection of PAC Binding Aptamers

To isolate PAC binding RNAs, an affinity chromatography resin was generated as previously described [25]. Briefly, a PAC was synthesized by solid-phase methods with the sequence Abu-Ser-Val-Acr-Arg (Abu-SVAcrR), where Abu is an aminobutyric acid linker and Acr is an acridine amino acid developed in our laboratory (**1**, Figure 2) [20]. After purification by HPLC, this compound was immobilized via a reductive amination reaction involving the N-terminal primary amine and a commercially available aldehyde-functionalized agarose resin (**2**, Figure 2).

We used a SELEX (*s*ystematic *e*volution of *l*igands by *ex*ponential enrichment) protocol to isolate RNA aptamers that bind the AbuSVAcrR resin from an initial pool of 75 nt RNAs containing a 30 nt sequence random region (Figure 3) [9, 26–28]. In each round, the RNA pool was allowed to bind PAC resin **2** described above, followed by washing the unbound RNAs and eluting those bound with soluble PAC **1**. To monitor the progress through selections, the percentage of RNA pool that bound to **2** was measured at each round. This number rose from under 0.1% in the first round to approximately 6% by the ninth round. The RNAs eluting from the resin **2** with soluble PAC **1** in round ten were collected and cloned (P aptamers). In addition, RNAs that remained on the agarose resin after the PAC elution step in round ten were removed using a 7 M urea solution heated to 65°C, and these RNAs were cloned independently (U aptamers). A total of 28 PAC binding aptamer clones were sequenced (14 P and 14 U), and among these, seven different sequences were represented (sequences **a–g**, Figure 3).

Secondary Structure Prediction and Structure Probing

The most stable secondary structures for the seven RNA aptamer sequences were predicted using *mfold* [29, 30]. To test the validity of these structures, the RNAs were cleaved with ribonucleases selective for certain secondary structure elements. Results of these experiments largely support the predicted structures for sequences **a–c** and **g** (see Supplemental Data at http://www.chembiol.com/cgi/content/full/10/7/663/DC1). For sequence **d**, two structures of similar stability were predicted that could not be distinguished from the structure probing. In addition, the randomized region in sequences **e** and **f** appeared to have evolved to be nearly complementary to the fixed sequence present for PCR amplification and T7 transcription. For these reasons, the three aptamers (**d**, **e**, and **f**) were not studied further. For sequences **a**, **b**, **c**, and **g**, the randomized region evolved to a self-complementary hairpin stem interrupted by a large internal loop (≥4 nt), with additional single nucleotide bulges present (Figure 4). Interestingly, in each of these structures, the sequence 5′-CGU-3′ is present in the stem with the 5′-C•G base pair closing the large internal loop.

Binding Site Identification with EDTA•Fe-PAC

We identified the binding sites for the PAC using affinity cleaving with EDTA•Fe-modified ligand (**3**, Figure 2). The

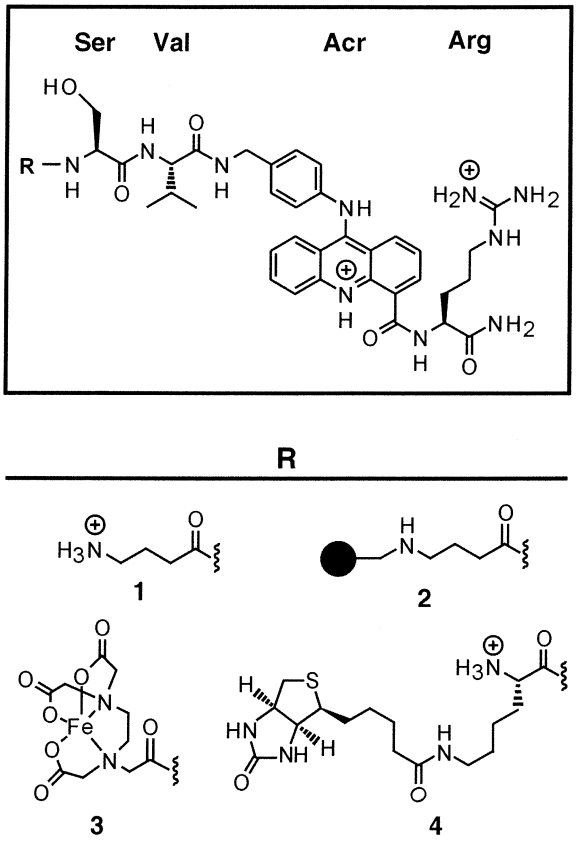

Figure 2. Chemical Structures of PAC Derivatives Used in This Study

The PAC Abu-Ser-Val-Acr-Arg **1** was prepared by SPPS and used to elute RNAs bound to the PAC resin **2** in the SELEX experiment. This PAC was also modified with EDTA•Fe and biotin to yield PACs **3** and **4**, respectively.

ability of the tethered EDTA•Fe to generate hydroxyl radicals and cleave RNA independent of sequence allows for unambiguous determination of the PAC binding site [31, 32]. The cleavage reagent **3** was prepared by coupling EDTA monoanhydride [33] to the amino terminus of the PAC SVAcrR while it was immobilized on the solid phase synthesis support. Subsequent side chain deprotection and cleavage from the support, HPLC purification, and addition of ferrous ion yields the PAC **3**. This compound efficiently cleaved nucleotides in the evolved sequences, identifying the binding sites for the PAC on the four aptamers studied (sequences **a**, **b**, **c**, and **g**) (Figure 4).

PAC binding sites on these RNAs have the common structural element containing the 5′-CGU-3′ sequence with the C and G base-paired, the U in a bulge or G•U wobble pair, and the 5′-C•G base pair adjacent to a loop or bulged nucleotide. From the number of nucleotides cleaved, it appears binding is less selective on the **b** and **c** aptamers. In addition to the 5′-CGU sequence, the **b** aptamer has 5′-CAU-3′ present in the stem immediately before the internal loop. In the **c** aptamer, the 5′-CGU-3′ sequence appears three times and 5′-CAU is also present in the evolved stem. These sequence elements may constitute additional binding sites for the PAC on these two RNAs.

Aptamers Bind the PAC with Different Affinities

The PAC binding affinities for the **a**, **b**, **c**, and **g** aptamers were estimated using a quantitative ribonuclease footprinting assay. For each RNA, PAC **1** (Figure 2) inhibited cleavage by ribonuclease V1 at nucleotides in the PAC binding site. This effect was measured as a function of PAC concentration and the data fit to generate a binding isotherm for each aptamer (Figure 5). Interestingly, the binding constants varied significantly for the different aptamers with the **g** sequence binding with the highest affinity (K_D = 21 nM) and the **b** sequence with the lowest (K_D = 770 nM). The **a** and **c** sequence aptamers bound the PAC with similar affinities (K_D = 145 nM and 90 nM, respectively). The magnitude of the measured dissociation constant for sequence **g** was also determined using a quantitative ribonuclease T1 footprinting assay. The results of this experiment are in good agreement with the V1 footprinting on this RNA (K_D = 20 nM) (Figure 5). The fact that the dissociation constants for the binding of **1** to the different aptamers vary by over 30-fold underscores the ability of this structure to discriminate among different RNA binding sites.

Minimal Binding Site from Sequence g Aptamer

The PAC binding site on the aptamer with the highest affinity (sequence **g**) was further characterized. The nucleotides cleaved by the EDTA•Fe-PAC **3** indicated the PAC binding site resides in the center of the RNA in a G•C-rich stem near a four nucleotide internal loop (Figure 4B). These results predict that much of the RNA sequence present in the 5′ and 3′ ends would be dispensable for binding site formation. To test this idea, we synthesized a 27 nt RNA lacking 25 nt from the 5′-end and 23 nt from the 3′-end of the original **g** sequence aptamer. To determine if the binding site was maintained, the 27-mer was cleaved with compound **3**. Im-

A

5′-GGGAGAGGAUACUACACGUG - $(N)_{30}$ - CCAUUGCAUGUAGCAGAAGCUUCCG-3′

B

RNA sequence	random region $(N)_{30}$	# of clones
a	GAGCAUGUACGUGCGGUAUGCCGAUUAUGC	7
b	AAUGGCAUCUCGUCCUUAUUGGCGCAGUGA	11
c	GUGUCGUCGUGUGAUCGUAACCGUACGCAU	1
d	CAAUAAGUUCGUCGAGGCAUUACGCGUUUG	5
e	UAUCCUCAGCGUUCUGCUACUGACGAUGUU	2
f	GCCUCUCCCCGCGACUCUGUUCAAUGCUAA	1
g	ACAGUGGGCGUCGGCUUCAACCGCGAAUUC	1

Figure 3. PAC Binding RNA Aptamers Identified in This Study

(A) Sequence of the initial RNA pool used for SELEX experiments. RNAs are 75 nt long with a 30 nt random region.

(B) Different RNA aptamers identified after 10 rounds of SELEX and the number of clones containing that aptamer sequence.

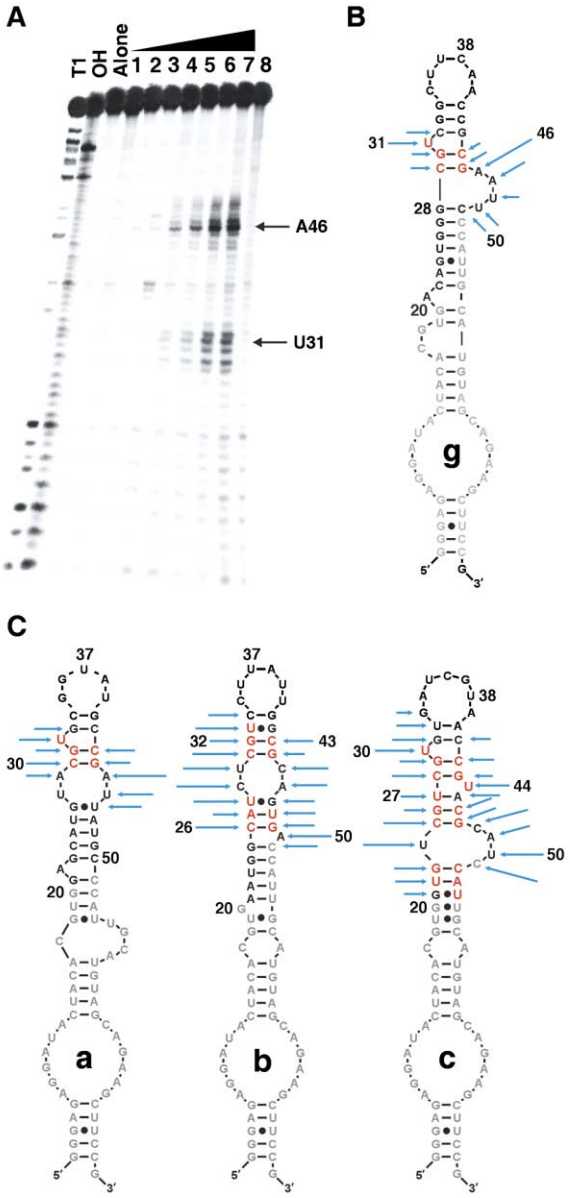

Figure 4. Characterization of Binding Sites on the RNA Aptamers

(A) Affinity cleavage of RNA aptamer sequence **g** using the EDTA•Fe-modified PAC **3**. Shown is a storage phosphor autoradiogram of a 10.5% denaturing polyacrylamide gel separating 5′-end-labeled RNA cleavage products. Major cleavage sites are near U31 and A46, and no other cleavage was observed. Structure probing: T1, RNase T1 (G lane); OH, alkaline hydrolysis; Alone, RNA in buffer only. Lanes 1–7, increasing concentrations of PAC **3** (0, 0.01, 0.1, 1, 3, 6, 10 μM) with 0.01% H_2O_2 and 5 mM DTT; lane 8, control with 10 μM SVAcrR and 10 μM free EDTA•Fe with 0.01% H_2O_2 and 5 mM DTT.

(B) Secondary structure of RNA sequence **g** as predicted by *mfold* [29, 30], with blue arrows identifying cleaved nucleotides and red letters comprising the putative binding site.

(C) Secondary structures, cleaved nucleotides, and possible binding sites for RNA sequences **a**, **b**, and **c**. See Experimental Procedures for more details.

portantly, the same nucleotides are cleaved on this RNA as was observed with the full-length **g** sequence aptamer, indicating similar binding on both RNAs (Figure 6).

Analysis of PAC-RNA Binding by SPR

Surface plasmon resonance (SPR) studies were used to explore the kinetics of PAC binding [34]. The PAC SVAcrR was modified at its N terminus with a commercially available ϵ-amino-biotinylated lysine residue to yield biotin-KSVAcrR (**4**, Figure 2). This compound was captured on a streptavidin-functionalized biosensor chip for monitoring binding. The sensorgram generated from the addition of various concentrations of the 27-mer RNA is shown in Figure 6C. These binding data were globally fit to a 1:1 interaction model to extract association and dissociation rate constants using the data analysis program CLAMP [35]. From this analysis, $k_a = 1.1 \times 10^4\ M^{-1}s^{-1}$ and $k_d = 1.7 \times 10^{-2}\ s^{-1}$, corresponding to a $K_D = 1.6$ μM for this RNA. For comparison, the full-length **g** sequence aptamer bound the PAC chip with $k_a = 5.3 \times 10^3\ M^{-1}s^{-1}$, $k_d = 6.9 \times 10^{-3}\ s^{-1}$, and $K_D = 1.3$ μM. Thus, the full-length aptamer and the 27-mer RNA bind with similar affinities and kinetics. It is interesting to note that binding affinity to the full-length aptamer is apparently lost by tethering the PAC to the chip surface ($K_D = 20$ nM by footprinting, $K_D = 1.3$ μM by SPR).

Since intercalating ligands also have the potential to bind DNA, we compared the binding of the PAC to the 27-mer RNA with its binding to a DNA duplex. This was accomplished using a short DNA duplex corresponding in sequence to that found in the base-paired region of the 27-mer RNA (Figure 6D). Binding of the DNA 22-mer to PAC **4** in SPR experiments required higher concentrations and displayed considerably different binding kinetics than observed with the RNA, indicating a different, weaker binding mode for this nucleic acid. Indeed, the K_D obtained from the fit of the kinetic data is nearly two orders of magnitude higher for the DNA (133 μM) than for the RNA 27-mer (1.5 μM). This is primarily due to the approximately 50-fold higher dissociation rate constant for the PAC DNA interaction ($k_d = 1\ s^{-1}$).

Discussion

Recently our laboratory and others have pursued the goal of developing a systematic approach to the discovery of small molecules capable of controlling the function of RNA targets in vivo [8, 21, 36–51]. We have focused our efforts on molecules with the potential to bind RNA in base-paired secondary structure via threading intercalation. Binding of this type of compound can be specific due to stabilizing interactions between substituents on the intercalator and functionality present in the grooves of the duplex or at bulged, mismatched, or looped nucleotides found adjacent to the intercalation site. In addition, this binding mode may be intrinsically selective for base-paired regions in RNA that are highly dynamic due to the necessity for base-pair opening to allow for threading to occur. The compounds currently under development by us for this purpose are peptide-acridine conjugates (PACs), wherein the acridine heterocycle is functionalized with peptide substituents at both the 4- and 9-positions (Figure 1A). Since no high-resolution structural data are available for complexes with intercalators bound to RNA beyond dinucleotides, a de-

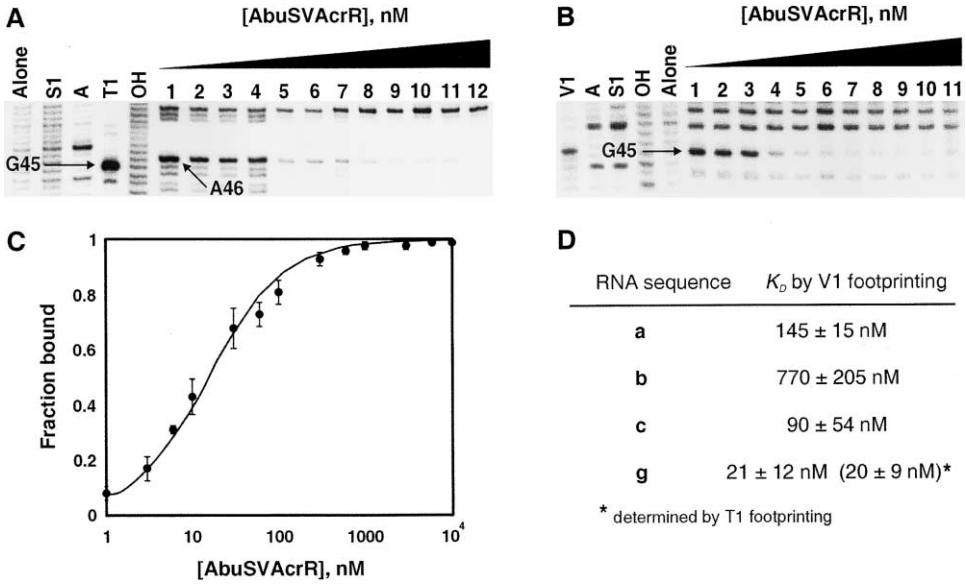

Figure 5. RNase Footprinting Analysis

(A) Quantitative ribonuclease V1 footprinting with PAC **1** and RNA sequence **g** aptamer. Shown is a partial storage phosphor autoradiogram of a 10.5% denaturing polyacrylamide gel separating 5′-end-labeled RNA cleavage products. Structure probing: Alone, RNA in buffer only; S1, S1 nuclease; A, RNase A; T1, RNase T1; OH, alkaline hydrolysis. Lanes 1–12, increasing concentrations of PAC **1** (0, 0.001, 0.003, 0.01, 0.03, 0.06, 0.1, 0.3, 1, 3, 6, 10 μM) in the presence of RNase V1.

(B) Quantitative ribonuclease T1 footprinting with PAC **1** and RNA sequence **g** aptamer. Shown is a partial storage phosphor autoradiogram of a 10.5% denaturing polyacrylamide gel separating 5′-end-labeled RNA cleavage products. Structure probing: V1, RNase V1; A, RNase A; S1, S1 nuclease; OH, alkaline hydrolysis; Alone, RNA in buffer only. Lanes 1–11, increasing concentrations of PAC **1** (0, 0.001, 0.01, 0.03, 0.1, 0.3, 1, 3, 10, 30, 100 μM) in the presence of RNase T1.

(C) Plot of fraction bound versus concentration of PAC **1** as determined by RNase V1 footprinting.

(D) Table of K_D values determined by RNase V1 and T1 footprinting.

sign/synthesis approach to selective, high-affinity ligands of this type is not currently feasible. One strategy we have investigated is to generate libraries of these molecules and screen the libraries with various RNAs from pathogenic organisms for ligands with high affinity and specificity [21]. To complement and guide these experiments, we endeavored here to discover preferred RNA binding sites for a representative PAC using in vitro evolution of the RNA (SELEX) [26]. The potential value in drug discovery efforts of using SELEX to identify RNA motifs predisposed to bind certain organic compounds has been discussed in the literature [27, 52–54]. The PACs are well suited for study via this approach because they are prepared by a simple, modular solid-phase synthesis making the generation of derivatives easy and rapid. Such derivatives include soluble PAC **1** and affinity matrix **2**, used during the selection, and compounds **3** and **4**, prepared for characterization of PAC-RNA complexes. Future structure/function studies to determine the origin of binding affinity and selectivity will also be facilitated by the simple, solid-phase PAC synthesis.

It appears the sequence 5′-C(G/A)U-3′, wherein the C and the purine are base-paired and the U is either bulged or in a G•U wobble, defines a binding site for the PAC SVAcrR. In addition, there is an apparent requirement for the 5′-C•G pair to be adjacent to a loop or bulge in the stem. This structure appears once in the **a** and **g** aptamers, twice in **b**, and four times in the **c** aptamer (Figure 4). The selectivity of cleavage by the EDTA•Fe PAC **3** is consistent with this definition since the most selective cleavage is observed with **a** and **g**, and least selective on **c** (Figure 4). The highest-affinity binding occurs with the **g** sequence where the 5′-C•G pair closes a four nucleotide asymmetric loop and the U is bulged (Figures 4 and 5).

Our current model for the PAC-RNA complex formed at these binding sites involves intercalation of the acridine at the 5′-CpG/A-3′ site. It is important to note that the base-paired region (5′-CpG/A-3′)•(3′-GpC/U-5′) is common to all the aptamer binding sites and the 5′-CpG-3′ step is a well-characterized intercalation site for acridines in duplex DNA [55]. Indeed, a recent crystal structure of a 9-aminoacridine-4-carboxamide bound to the DNA sequence $(5'\text{-CGTACG-}3')_2$ showed the acridine intercalated at both CpG steps with the 4-carboxamide substituent making major groove contacts to the G [56, 57]. However, acridines do not bind exclusively to CpG steps. Indeed, another structure of an acridine derivative substituted at the 9-position with a tetraarginine peptide has been reported with the acridine bound at the ApA step in the DNA sequence 5′-CGCGAATTC GCG-3′ [58]. Also, acridines have been shown to bind to TAR RNA and U1A RNA in locations that do not contain the CpG sequence [47, 59]. Thus, we could not have predicted a priori that we would observe such a predominance of base-paired 5′-CpG-3′ steps in RNAs selected against a peptide-acridine conjugate in such an unbiased experiment. This study is the first of its kind to use RNA selection experiments to determine preferred binding sites for a known intercalating ligand.

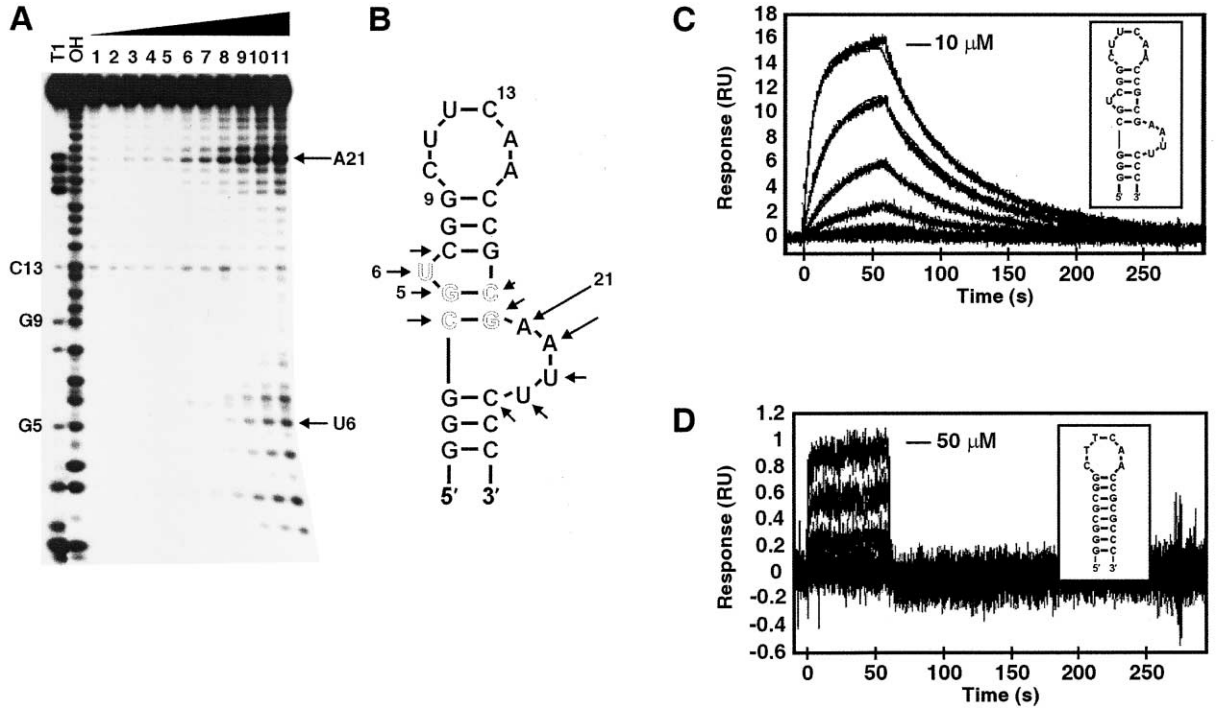

Figure 6. Characterization of the Binding to 27-mer RNA Derived from Sequence g Aptamer

(A) Storage phosphor autoradiogram of a 20% denaturing polyacrylamide gel separating 5′-end-labeled RNA cleavage products. Structure probing: T1, RNase T1 (G lane); OH, alkaline hydrolysis. Lane 1, control with 30 μM SVAcrR and 30 μM free EDTA•Fe with 0.01% H_2O_2 and 5 mM DTT; lane 2, RNA alone (in buffer only); lanes 3–11, increasing concentrations of PAC **3** (0.01, 0.1, 0.3, 0.6, 1, 3, 6, 10, and 30 μM) with 0.01% H_2O_2 and 5 mM DTT. A21 is the most efficiently cleaved nucleotide (analogous to A46 in the full length RNA sequence **g**).

(B) Secondary structure of the 27-mer RNA as predicted by *mfold* [30, 31]. Black arrows identify cleaved nucleotides and outlined letters indicate the putative binding site.

(C) SPR sensorgram for a 3-fold dilution series of 27-mer RNA binding to PAC **4** immobilized onto a streptavidin-coated biosensor chip starting with 10 μM.

(D) SPR sensorgram of a 3-fold dilution series of 22-mer DNA starting with 50 μM. Overlayed on these sensorgrams is the curve fit as determined by the data analysis program CLAMP [36].

The results shed new light on the value this sequence in RNA as a PAC binding site, underscoring the importance of targeting naturally occurring RNAs that have the CpG sequence with these compounds.

Importantly, the 5′-CpG-3′ sequence itself does not define the PAC binding site. In each of the PAC binding aptamers, the base-paired 5′-CpG-3′ structure is sandwiched between non-Watson-Crick elements. Indeed, a U always flanks this sequence on the 3′ side, typically in a single base bulge or G•U pair. Furthermore, a C•G pair closes a large internal loop (>4 nt) in each of the selected RNAs. The nature of the non-Watson-Crick structure in the aptamers plays a significant role in determining affinity as the dissociation constants for PAC binding vary over 30-fold. The highest-affinity site contains a base-paired 5′-CpG-3′ step flanked on the 5′ side by a 4 nt internal loop and the 3′ side by a bulged U. The presence of the loops and bulges likely affects the base-pair dynamics at this site, rendering the intercalation site accessible to a potential threading intercalator like SVAcrR. Furthermore, in acridine intercalation complexes, significant unwinding of the helix is observed at the intercalation site with overwinding at the adjacent base pair. Distortion from the ground state helical structure necessary to allow for intercalation may be facilitated in an RNA binding site with the CpG step adjacent to nonhelical secondary structure. A similar explanation was used to rationalize why single base bulges in an RNA duplex facilitates ethidium bromide intercalation at a CpG step [60]. It is also possible that direct contacts are made between the substituents on the acridine ring and nucleotides found in the loops and bulges. Additional studies will be necessary to determine the relative importance of direct contacts between the acridine substituents and looped or bulged nucleotides and the effects these structures have on RNA conformational flexibility. These efforts will benefit from the observation that the binding site found in the 75 nt sequence **g** aptamer can be localized to a 27 nt stem-loop structure (Figure 6).

The biotinylated PAC **4** bound weakly to a G•C-rich DNA duplex, with the lower binding affinity a consequence of significantly faster dissociation rate than observed with the 27-mer RNA (Figure 6). Acridine intercalators, such as proflavine, have been shown to bind DNA in a two-step mechanism, rapidly forming an initial "outside" or "groove bound" complex prior to formation of the more stable intercalation complex [61]. The outside complex formed with proflavine and calf thymus DNA dissociates approximately 40 times faster than

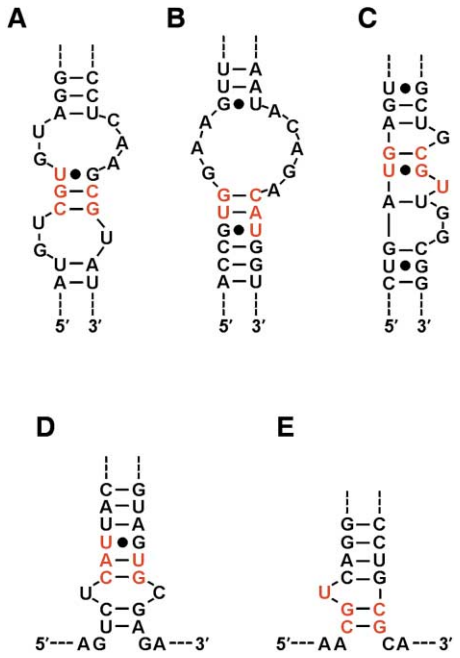

Figure 7. Secondary Structures within Untranslated Regions of Viral Genomes Containing a Putative PAC Binding Site

Structures originate from (A) IRES element in the 5′-UTR of EMCV (strain B) [62]; (B) 5′-UTR of CVB3 (strain Nancy) [63]; (C) 5′-UTR of CAV2 [64]; (D) 3′-UTR of TEV [65]; and (E) 3′-UTR of JE virus [66]. Putative PAC binding sites have been highlighted in red.

does the intercalation complex [61]. Thus, the weak PAC binding observed with the DNA duplex may be due to an outside, nonintercalative binding mode. Moreover, the bulky peptide substituents at the 4- and 9-positions on the acridine likely prevent insertion between the base pairs of the DNA duplex. Similar hindered binding has been observed previously with a derivative of proflavine with bulky substituents. 2,7-Di-*t*-butylproflavine is only capable of forming the "outside" complex with DNA and does not intercalate [62].

The SELEX experiments described here have provided RNA structures that will continue to help us understand the RNA recognition properties of PACs. In addition, the definition of preferred binding sites that comes from analysis of the SELEX results can be used to guide the choice of naturally occurring target RNAs for screens against PAC libraries. We analyzed the published secondary structures for several viral 5′- and 3′-untranslated region (UTR) sequences to determine if structures that fit the criteria for a preferred binding site for the PAC were present. Viral UTRs contain key regulatory elements, often including an internal ribosomal entry site (IRES) responsible for initiating translation of the viral genome [63]. Thus, the binding of a small molecule to structure found in the UTR may have a detrimental effect on viral replication. In structures predicted for the 5′-UTRs from encephalomyocarditis virus [64], coxsackievirus B3 [65], and coxsackievirus A2 [66] and 3′ UTRs for tobacco etch virus [67] and Japanese encephalitis [68] we found five potential PAC binding sites (Figures 7A–7E, respectively). In each case, the sequence 5′-C(A/G)U-3′ is present with the C and the purine base-paired, the U in a bulge or G•U wobble pair, and the 5′-C•G pair adjacent to an internal loop. Future experiments will determine if any of these sites are predisposed for PAC binding. If so, the RNA will become a good candidate for screens against combinatorial libraries of PAC derivatives to increase binding affinity and selectivity.

Significance

Unbiased RNA selection experiments were used in this study to determine preferred binding sites for a peptide-acridine conjugate (PAC). In each of the RNA aptamers studied, a PAC binding site contains a base-paired 5′-CpG-3′ step, a known acridine intercalation site. These results shed new light on the value of the 5′-CpG-3′ step in RNA as a PAC binding site, underscoring the importance of targeting naturally occurring RNAs that contain this structure with these compounds. However, one of the most important observations in this study is that the 5′-CpG-3′ step itself does not define a preferred site for this PAC. Indeed, we have shown that a DNA duplex containing two 5′-CpG-3′ steps binds with a K_D two orders of magnitude higher than does the high-affinity aptamer. The presence and nature of flanking non-Watson-Crick structure play significant roles in determining affinity. The preferred site (K_D = 20 nM) contains a 5′-CpG-3′ step flanked on the 5′ side by a 4 nt internal loop and the 3′ side by a bulged U. This information is critical in identifying possible PAC binding sites in naturally occurring RNAs and guiding future selections from PAC libraries to optimize affinity and selectivity. Indeed, using site selection criteria defined by these experiments, potential PAC binding sites have been identified in the published secondary structures of 5′- and 3′-UTRs from several viruses. In addition, the identification of a small RNA (27 nt) that binds well to the PAC sets the stage for high-resolution structural studies that will aid in defining the basis for the binding selectivity observed.

Experimental Procedures

General

Distilled, deionized water was used for all aqueous reactions and dilutions. All reagents were obtained from Sigma/Aldrich unless otherwise noted. Restriction enzymes and nucleic acid-modifying enzymes were purchased from New England Biolabs unless otherwise noted. Oligonucleotides were prepared on a Perkin Elmer/ABI Model 392 DNA/RNA synthesizer with β-cyanoethyl phophoramidites. 5′-Dimethoxytrityl (DMT)-protected 2′-deoxyadenosine, 2-deoxyguanosine, 2′-deoxycytidine, and thymidine phosphoramidites were purchased from Perkin Elmer/ABI. 2′-O-Tertbutyldimethylsilyl (2′-O-TBDMS) protected adenosine, guanosine, cytidine, and uridine. Ribonucleoside phosphoramidites were purchased from Glen Research. [γ-^{32}P]ATP and [α-^{32}P]ATP (6000 Ci/mmol) was obtained from DuPont NEN. Storage phosphor autoradiography was carried out using imaging plates purchased from Kodak. A Molecular Dynamics STORM 840 and ImageQuant 5.2 software (Molecular Dynamics) were used to obtain and analyze all data from phosphor imaging plates, respectively.

Synthesis of PAC Derivatives 1-4

All PACs were synthesized using 9-fluoronylmethoxycarbonyl (Fmoc)-protected amino acids (NovaBiochem) on Rink Amide MBHA

resin (NovaBiochem; 0.72 mmol/g loading) according to standard SPPS protocols [69, 70]. Use of the 9-anilinoacridine amino acid has been previously described [20]. The PAC sequence Abu-Ser-Val-Acr-Arg (**1**) was cleaved from the solid-phase synthesis support with Reagent B (TFA/TIS/H_2O/phenol [90:5:2.5:2.5]). The resulting solution was evaporated in vacuo and extracted between water and diethyl ether. The acid aqueous layer was neutralized with triethylamine and then concentrated by lyophilization. HPLC-purification (to >95%) was performed on a reverse-phase C18 column (4.6 × 250 mm, Vvdac) over 30 min with a flow rate of 1.5 ml/min. Compound **1** was analyzed by electrospray mass spectrometry (ESI-MS) on a Thermo Finnigan LC-Q Duo (San Jose, CA) instrument as previously described [19]. Calculated mass for **1**, 769.4; Found $[M+H]^+$, 770.5 *m/z*. Stock solutions of all PACs were prepared to uniform UV absorbance (λ = 442 nm) assuming a calculated extinction coefficient of 6000 $M^{-1}\cdot cm^{-1}$.

The covalent attachment of a soluble PAC to commercially available aldehyde-functionalized agarose (PAC resin **2**) has also been described [25]. Briefly, the PAC was prepared for immobilization to AminoLink® Plus Coupling Gel (Pierce) by dilution of a stock solution with pH 10 coupling buffer and addition of this mixture to the equilibrated gel slurry. Reductive amination was achieved using sodium cyanoborohydride. The remaining unreacted aldehyde sites on the resin were blocked with a 1 M Tris buffer and subsequently reduced. The substitution of the PAC on the agarose resin used for SELEX experiments was 0.5 μmol per ml (or 0.5 mM).

The EDTA•Fe-modified PAC **3** for affinity cleavage and the biotinylated PAC **4** for SPR experiments were also prepared by SPPS. The solid supported sequence Ser-Val-Acr-Arg was allowed to react with EDTA monoanhydride [33] or activated Fmoc-Lys(Biotin)-OH (Advanced ChemTech) in anhydrous DMF. The resulting PACs were deprotected, cleaved from the support, purified by HPLC, and characterized by ESI-MS as described above. Calculated mass for **3** (without iron), 958.4; Found $[M+H]^+$, 959.4 *m/z*. A 2-fold excess of ammonium ferrous sulfate was added to an aqueous solution of the EDTA-PAC to load it with iron. This compound was used for all affinity cleavage experiments. Calculated mass for **4**, 1038.5; Found $[M+H]^+$, 1039.7 *m/z*.

Random Library Preparation

A 75 nt DNA oligonucleotide (0.2 nmol) was used as the template for a three-cycle PCR reaction, which yielded a 100 bp dsDNA product consisting of a T7 promoter and a 30-mer random region flanked by EcoRI and HindIII cloning sites. Transcription from this DNA with T7 RNA polymerase generated a pool of 75 nt-long RNA molecules. [α-^{32}P]ATP was used to body label the RNA pool for each round of selection.

SELEX

In each round, ~2 nmol of the RNA pool was denatured at 95°C in 0.5 ml of the selection buffer (1× SB: 50 mM Bis-Tris•HCl, 100 mM NaCl, 10 mM $MgCl_2$ [pH 7.0]) and allowed to slowly cool to room temperature. The RNA pool was added to 100 μl of Tris-capped resin (preclear) and allowed to incubate for 30 min in order to exclude resin binding RNAs. The RNAs that did not bind the preclear resin were incubated with 100 μl of PAC resin **2** for 1 hr, followed by washing 10 times with 1 ml of wash buffer (1× SB with additional 200 mM NaCl) to remove nonbinding RNAs. Bound RNAs were eluted by incubating the beads with 1 ml of 1 mM soluble PAC **1** for 30 min. The eluted RNAs were rid of compound **1** using dialysis, then treated with 5 units of RNase-free DNase I (Promega) for 3 hr at 37°C. Access RT-PCR kit (Promega) was used to amplify RNA winners from each round. The progress of selections was monitored by calculating the percent of input RNA that was retained by PAC resin **2** after the washing steps. This was accomplished by measuring the counts per min of the two respective RNA pools (input and bound RNA).

Cloning

The cDNA from the final round was digested with EcoRI and HindIII, then cloned into pUC-19 plasmids and transformed into *E. coli* XL-1 Blue cells (Stratagene). Plasmids coding for individual RNA clones were isolated, sequenced (U of Utah Health Sciences DNA sequencing facility), and used for subsequent production of RNA aptamers.

RNA Synthesis and End-Labeling

All 75 nt RNA aptamers were generated by run-off transcription with T7 RNA polymerase. First, 100-mer dsDNA PCR products were amplified from pUC-19 plasmids using 25-mer and 45-mer DNA oligonucleotide primers. Sequences are as follows: 25-mer, 5′-CGG*AAGCTT*CTGCTACATGCAATGG-3′, the HindIII restriction site is italicized; 45-mer, 5′-GCG*AATTC*TAATACGACTCACTCTCGGGAGAGGATACTACACGTG-3′, the EcoRI restriction site is italicized and the T7 promoter is underlined. The PCR product was extracted with phenol/chloroform, ethanol precipitated, redissolved in 100 μl reaction volumes consisting of transcription buffer [71], DTT (10 mM), NTPs (2 mM each), and RNasin (Amersham Pharmacia) and incubated with T7 RNA polymerase at 40°C overnight. The reaction mixture was treated with RNase-free DNase I (Promega) for 3 hr at 37°C. RNA aptamers were purified on a 10.5% denaturing polyacrylamide gel. Bands were visualized by UV shadowing and excised from the gel, followed by overnight elution via the crush and soak method [71]. After filtration, the resulting solution was extracted with phenol/chloroform, ethanol precipitated, and the RNA concentration was determined by measuring the absorbance at 260 nm. For the preparation of 5′-end-labeled RNA, 200 pmol of the transcript was first treated with shrimp alkaline phosphatase (SAP, Amersham Pharmacia) for 2 hr at 37°C. SAP-treated RNA was gel purified and isolated as described above. The dephosphorylated RNA was end-labeled using T4 polynucleotide kinase and [γ-^{32}P]ATP for 1 hr at 37°C. Labeled RNA aptamers were gel purified and isolated as described above. 27-mer RNA was chemically synthesized and deprotected with NH_3-saturated methanol for 24 hr at room temperature, followed by 0.1 M tetrabutylammonium fluoride (TBAF) in THF for 48 hr at room temperature. Deprotected RNA was purified on a 20% denaturing gel and end-labeled as described above. The HPLC-purified 22-mer DNA (U of Utah Health Sciences DNA/Peptide facility) was obtained >95% pure.

Secondary Structure Prediction and Structure Probing

Secondary structure prediction of all RNA sequences was performed using the web-based program *mfold* (version 3.1) developed by Dr. Michael Zuker [29, 30]. Probing of the predicted structure was accomplished by digesting the RNAs with 0.01 U RNase A (Ambion), 1 U nuclease S1 (Amersham Pharmacia), 2 U RNase T1 (USB), and 0.1 U RNase V1 (Pierce). Reactions were carried out for 1 to 15 min at room temperature in 1× SB under native (nondenaturing) conditions and in the presence of 10 μg/ml of yeast $tRNA^{phe}$. In the case of nuclease S1, reactions were supplied with 0.1 mM $ZnCl_2$ for optimal activity. Cleavage reactions were quenched with an equal volume of formamide loading dye, heat denatured, and analyzed by (10.5% or 20%) denaturing polyacrylamide gel electrophoresis.

PAC EDTA•Fe Cleavage Experiments

PAC-RNA complexes were formed by incubating varying concentrations of PAC **3** with ~5 nM end-labeled RNA for 15 min in 1× SB and 10 μg/ml of yeast $tRNA^{phe}$. The resulting complexes were probed by initiating hydroxyl radical formation with the addition of 0.01% H_2O_2 and 5 mM DTT, followed by incubation at room temperature for 30 min. Affinity cleaving reactions were quenched by the addition of 180 μl of distilled H_2O, followed by phenol/chloroform extraction and ethanol precipitation. Cleaved RNA was resuspended in formamide loading dye, heat denatured, and analyzed by (10.5% or 20%) denaturing polyacrylamide gel electrophoresis.

Quantitative Footprinting

Footprints for PAC **1** on RNA aptamers were obtained using RNase V1 and RNase T1 under native conditions. PAC-RNA complexes were formed by incubating increasing concentrations of PAC **1** with ~1 nM end-labeled RNA for 15 min in 1× SB and 10 μg/ml of yeast $tRNA^{phe}$. Reactions were initiated by 5 min enzymatic digestions with 0.1 U RNase V1 or 2 U RNase T1, followed by quenching with formamide loading dye. Cleaved RNA was heat denatured and analyzed by 10.5% denaturing polyacrylamide gel electrophoresis. The cleavage efficiency at nucleotide(s) near the binding site was calculated by normalizing for the differential loading for each concentration of PAC **1** tested. For the RNA sequence **g** aptamer, the footprint of A46 cleaved by RNase V1 was monitored with respect to the V1-

dependent constant band U54. For the RNase T1 footprint, the cleavage efficiency at G45 was monitored with respect to C50. Similar nucleotides were monitored for quantitative RNase V1 footprinting of sequence **a**, **b**, and **c** aptamers (see Supplemental Data at http://www.chembiol.com/cgi/content/full/10/7/663/DC1). The cleavage data for each RNA was converted to binding data for PAC **1**, assuming that the maximum cleavage efficiency corresponds to 0% occupancy by the PAC and the minimum cleavage efficiency corresponds to 100% occupancy by the PAC. The fraction of RNA aptamer bound by PAC **1** was plotted as a function of concentration, and the data were fitted to the equation: fraction bound = [PAC **1**]/[PAC **1**] + K_D. The results are reported as the average and standard deviation for at least three different experiments.

Surface Plasmon Resonance

All binding studies were carried out on a Biacore S51 biosensor (Biacore AB, Uppsala, Sweden). Approximately 4000 RU of streptavidin was immobilized onto a Pioneer Chip B1 using standard amine coupling chemistry. A biotinylated form of SVAcrR **4** was captured onto the streptavidin surface at a density of ~10 RU. RNA and DNA analyte samples were injected over the SVAcrR and control surfaces at a flow rate of 90 μl/min. Bound complexes were dissociated with a 10 s wash with 2.5 M guanidine HCl. Each analyte sample was injected twice to demonstrate the reproducibility of the assay. All data were processed by subtracting out the response from the reference spot, along with subtracting out an average of 6 blank injections. The responses were also normalized by the molecular mass of each analyte. The resulting data were globally fit using a 1:1 interaction model in order to determine the reaction rate constants. The entire analysis was repeated to determine the reproducibility in reaction parameters. The k_a, k_d, and K_D values were reproducible to within ±30%.

Acknowledgments

We would like to thank David G. Myszka at the Center for Biomolecular Interaction Analysis at the University of Utah (http://www.cores.utah.edu/interaction) for performing all SPR biosensor experiments. P.A.B. acknowledges financial support from the NIH (AI-49062) and a Camille Dreyfus Teacher Scholar Award. B.D.G. was supported by a National Institutes of Health training grant (GM-08573).

Received: April 17, 2003
Revised: June 3, 2003
Accepted: June 9, 2003
Published: July 18, 2003

References

1. Pearson, N.D., and Prescott, C.D. (1997). RNA as a drug target. Chem. Biol. *4*, 409–414.
2. Hermann, T., and Westhof, E. (1998). RNA as a drug target: chemical, modeling, and evolutionary tools. Curr. Opin. Biotechnol. *9*, 66–73.
3. Wilson, W.D., and Li, K. (2000). Targeting RNA with small molecules. Curr. Med. Chem. *7*, 73–98.
4. Xavier, K.A., Eder, P.S., and Giordano, T. (2000). RNA as a drug target: methods for biophysical characterization and screening. Trends Biotechnol. *18*, 349–356.
5. Gallego, J., and Varani, G. (2001). Targeting RNA with small-molecule drugs: therapeutic promise and chemical challenges. Acc. Chem. Res. *34*, 836–843.
6. Gilman, A.G., Rall, T.W., Nies, A.S., and Taylor, P. (1990). Goodman and Gilman's The Pharmacological Basis of Therapeutics, Eighth Edition (New York: McGraw-Hill).
7. Moazed, D., and Noller, H.F. (1987). Interaction of antibiotics with functional sites in 16S ribosomal RNA. Nature *327*, 389–394.
8. Werstuck, G., and Green, M.R. (1998). Controlling gene expression in living cells through small molecule-RNA interactions. Science *282*, 296–298.
9. Vuyisich, M., and Beal, P.A. (2002). Controlling protein activity with ligand-regulated RNA aptamers. Chem. Biol. *9*, 907–913.
10. Chow, C.S., and Bogdan, F.M. (1997). A structural basis for RNA-ligand interactions. Chem. Rev. *97*, 1489–1513.
11. Michael, K., and Tor, Y. (1998). Designing novel RNA binders. Chem. Eur. J. *4*, 2091–2098.
12. Wilson, W.D., and Jones, R.L. (1981). Intercalating drugs: DNA binding and molecular pharmacology. Adv. Pharmacol. Chemother. *18*, 177–222.
13. Wilson, W.D., Ratmeyer, L., Zhao, M., Strekowski, L., and Boykin, D. (1993). The search for structure-specific nucleic acid-interactive drugs: effects of compound structure on RNA versus DNA interaction strength. Biochemistry *32*, 4098–4104.
14. Nonin, S., Jiang, F., and Patel, D.J. (1997). Imino proton exchange and base-pair kinetics in the AMP-RNA aptamer complex. J. Mol. Biol. *268*, 359–374.
15. Liaw, Y.-C., Gao, Y.-G., Robinson, H., van der Marel, G.A., van Boom, J.H., and Wang, A.H.-J. (1989). Antitumor drug nogalamycin binds DNA in both grooves simultaneously: molecular structure of nogalamycin-DNA complex. Biochemistry *28*, 9913–9918.
16. Jourdan, M., Garcia, J., and Lhomme, J. (1999). Threading bis-intercalation of a macrocyclic bisacridine a abasic sites in DNA: nuclear magnetic resonance and molecular modeling study. Biochemistry *38*, 14205–14213.
17. Guelev, V., Lee, J., Ward, J., Sorey, S., Hoffman, D.W., and Iverson, B.L. (2001). Peptide bis-intercalator binds DNA via threading mode with sequence specific contacts in the major groove. Chem. Biol. *8*, 415–425.
18. Ryter, J.M., and Schultz, S.C. (1998). Molecular basis of double-stranded RNA-protein interactions: structure of a dsRNA-binding domain complexed with dsRNA. EMBO J. *17*, 7505–7513.
19. Carlson, C.B., and Beal, P.A. (2000). Solid-phase synthesis of acridine-peptide conjugates and their analysis by tandem mass spectrometry. Org. Lett. *2*, 1465–1468.
20. Carlson, C.B., and Beal, P.A. (2000). Solid-phase synthesis of acridine-based threading intercalator peptides. Bioorg. Med. Chem. Lett. *10*, 1979–1982.
21. Carlson, C.B., Spanggord, R.J., and Beal, P.A. (2002). Selection of small-molecule mediators of the RNA regulation of PKR, the RNA-dependent protein kinase. Chembiochem *3*, 859–865.
22. Bailly, C., Colson, P., Houssier, C., and Hamy, F. (1996). The binding mode of drugs to the TAR RNA of HIV-1 studied by electric linear dichroism. Nucleic Acids Res. *24*, 1460–1464.
23. Cruse, W.B.T., Saludjian, P., Leroux, Y., Léger, G., El Manouni, D., and Prangé, T. (1996). A contiguous transition from A-DNA to B-DNA in the 1:1 complex between nogalamycin and the hexamer dCCCGGG. J. Biol. Chem. *271*, 15558–15567.
24. Sim, S.-P., Pilch, D.S., and Liu, L.F. (2000). Site-specific topoisomerase I-mediated DNA cleavage induced by nogalamycin: a potential role of ligand-induced DNA bending at a distal site. Biochemistry *39*, 9928–9934.
25. Carlson, C.B., and Beal, P.A. (2002). Point of attachment and sequence of immobilized peptide-acridine conjugates control affinity for nucleic acids. J. Am. Chem. Soc. *124*, 8510–8511.
26. Tuerk, C., and Gold, L. (1990). Systematic evolution of ligands by exponential enrichment: RNA ligands to bacteriphage T4 DNA polymerase. Science *249*, 505–510.
27. Ellington, A.D., and Szostak, J.W. (1990). In vitro selection of RNA molecules that bind specific ligands. Nature *346*, 818–822.
28. Ciesiolka, J., Illangasekare, M., Majerfeld, I., Nickles, T., Welch, M., Yarus, M., and Zinnen, S. (1996). Affinity selection-amplification from randomized ribooligonucleotide pools. Methods Enzymol. *267*, 315–335.
29. Zuker, M., Mathews, D.H., and Turner, D.H. (1999). Algorithms and Thermodynamics for RNA Secondary Structure Prediction: A Practical Guide in RNA Biochemistry and Biotechnology (Dordrecht: Kluwer Academic Publishers).
30. Mathews, D.H., Sabrina, J., Zuker, M., and Turner, D.H. (1999). Expanded sequence dependence of thermodynamic parameters improves prediction of RNA secondary structure. J. Mol. Biol. *288*, 911–940.
31. Schultz, P.G., Taylor, J.S., and Dervan, P.B. (1982). Design and synthesis of a sequence-specific DNA cleaving molecule: (distamycin-EDTA)iron(II). J. Am. Chem. Soc. *104*, 6861–6863.
32. Joseph, S., Whirl, M.L., Kondo, D., Noller, H.F., and Altman, R.B.

(2000). Calculation of the relative geometry of tRNAs in the ribosome from directed hydroxyl-radical probing data. RNA *6*, 220–232.

33. Ebright, Y.W., Chen, Y., Pendergrast, P.S., and Ebright, R.H. (1992). Incorporation of an EDTA-metal complex at a rationally selected site within a protein: application to EDTA-iron DNA affinity cleaving with catabolite gene activator protein (CAP) and Cro. Biochemistry *31*, 10664–10670.
34. Myszka, D.G. (1997). Kinetic analysis of macromolecular interactions using surface plasmon resonance. Curr. Opin. Biotechnol. *8*, 50–57.
35. Myszka, D.G., and Morton, T.A. (1998). CLAMP: a biosensor kinetic data analysis program. Trends Biochem. Sci. *23*, 149–150.
36. Yu, L., Oost, T.K., Schkeryantz, J.M., Yang, J., Janowick, D., and Fesik, S.W. (2003). Discovery of aminoglycoside mimetics by NMR-based screening of *Escherichia coli* A-site RNA. J. Am. Chem. Soc. *125*, 4444–4450.
37. Hamy, F., Felder, E.R., Heizmann, G., Lazdins, J., Aboul-ela, F., Varani, G., Karn, J., and Klimkait, T. (1997). An inhibitor of the Tat/TAR RNA interaction that effectively suppresses HIV-1 replication. Proc. Natl. Acad. Sci. USA *94*, 3548–3553.
38. Mei, H.-Y., Mack, D.P., Galan, A.A., Halim, N.S., Heldsinger, A., Loo, J.A., Moreland, D.W., Sannes-Lowery, K.A., Sharmeen, L., Truong, H.N., et al. (1997). Discovery of selective, small-molecule inhibitors of RNA complexes. I. The Tat protein/TAR RNA complexes required for HIV-1 transcription. Bioorg. Med. Chem. *5*, 1173–1184.
39. Tan, R., and Frankel, A.D. (1998). A novel glutamine-RNA interaction identified by screening libraries in mammalian cells. Proc. Natl. Acad. Sci. USA *95*, 4247–4252.
40. Wong, C.-H., Hendrix, M., Manning, D.D., Rosenbohm, C., and Greenburg, W.A. (1998). A library approach to the discovery of small molecules that recognize RNA: use of 1,3-hydroxamine motif as a core. J. Am. Chem. Soc. *120*, 8319–8327.
41. Hwang, S., Tamilarasu, N., Ryan, K., Huq, I., Richter, S., Still, W.C., and Rana, T.M. (1999). Inhibition of gene expression in human cells through small molecule-RNA interactions. Proc. Natl. Acad. Sci. USA *96*, 12997–13002.
42. Tok, J.B.-H., Cho, J., and Rando, R.R. (1999). Aminoglycoside antibiotics are able to specifically bind the 5′-untranslated region of thymidylate synthase messenger RNA. Biochemistry *38*, 199–206.
43. Luedtke, N.W., and Tor, Y. (2000). A novel solid-phase assembly for identifying potent and selective RNA ligands. Angew. Chem. Int. Ed. Engl. *39*, 1788–1790.
44. Takahashi, T., Hamasaki, K., Ueno, A., and Mihara, H. (2001). Construction of peptides with nucleobase amino acids: design and synthesis of the nucleobase-conjugated peptides derived from HIV-1 Rev and their binding properties to HIV-1 RRE RNA. Bioorg. Med. Chem. *9*, 991–1000.
45. Tok, J.B.-H., and Fenker, J. (2001). Novel synthesis and RNA-binding properties of aminoglycoside dimers conjugated via napthalene diimide-based intercalator. Bioorg. Med. Chem. Lett. *11*, 2987–2991.
46. Xiao, G., Kumar, A., Li, K., Rigl, T., Bajic, M., Davis, T.M., Boykin, D.W., and Wilson, W.D. (2001). Inhibition of the HIV-1 Rev-RRE complex formation by unfused aromatic cations. Bioorg. Med. Chem. *9*, 1097–1113.
47. Gayle, A.Y., and Baranger, A.M. (2002). Inhibition of the U1A-RNA complex by an aminoacridine derivative. Bioorg. Med. Chem. Lett. *12*, 2839–2842.
48. Harvey, I., Garneau, P., and Pelletier, J. (2002). Inhibition of translation by RNA-small molecule interactions. RNA *8*, 452–463.
49. Simonsen, K.B., Ayida, B.K., Vourloumis, D., Takahashi, M., Winters, G.C., Barluenga, S., Qamar, S., Shandrick, S., Zhao, Q., and Hermann, T. (2002). Novel paromamine derivatives exploring shallow-groove recognition of ribosomal-decoding-site RNA. Chembiochem *3*, 1223–1228.
50. Swayze, E.E., Jefferson, E.A., Sannes-Lowery, K.A., Blyn, L.B., Risen, L.M., Arakawa, S., Osgood, S.A., Hofstadler, S.A., and Griffey, R.H. (2002). SAR by MS: a ligand based technique for drug lead discovery against structured RNA targets. J. Med. Chem. *45*, 3816–3819.
51. Russell, R.J.M., Murray, J.B., Lentzen, G., Haddad, J., and Mobashery, S. (2003). The complex of a designer antibiotic with a model aminoacyl site of the 30S ribosomal subunit revealed by X-ray crystallography. J. Am. Chem. Soc. *125*, 3410–3411.
52. Osborne, S.E., and Ellington, A.D. (1997). Nucleic acid selection and the challenge of combinatorial chemistry. Chem. Rev. *97*, 349–370.
53. Famulok, M. (1999). Oligonucleotide aptamers that recognize small molecules. Curr. Opin. Struct. Biol. *9*, 324–329.
54. Hermann, T., and Patel, D.J. (2000). Adaptive recognition by nucleic acid aptamers. Science *287*, 820–825.
55. Adams, A. (2002). Crystal structures of acridines complexed with nucleic acids. Curr. Med. Chem. *9*, 1667–1675.
56. Todd, A.K., Adams, A., Thorpe, J.H., Denny, W.A., Wakelin, L.P.G., and Cardin, C.J. (1999). Major groove binding and 'DNA-induced' fit in the intercalation of a derivative of the mixed topoisomerase I/II poison *N*(-(2-dimethylamino)-ethyl)acridine-4-carboxamide (DACA) into DNA: X-ray structure complexed to d(CG(5Br-U)ACG)2 at 1.3-Å resolution. J. Med. Chem. *42*, 536–540.
57. Adams, A., Guss, J.M., Collyer, C.A., Denny, W.A., and Wakelin, L.P.G. (1999). Crystal structure of the topoisomerase II poison 9-amino-[*N*-(2-dimethylamino)ethyl]acridine-4-carboxamide bound to the DNA hexanucleotide $d(CGTACG)_2$. Biochemistry *38*, 9221–9233.
58. Malinina, L., Soler-López, M., Aymamî, J., and Subirana, J.A. (2002). Intercalation of an acridine-peptide drug in an AA/TT base step in the crystal structure of $[d(CGCGAATTCGCG)]_2$ with six duplexes and seven Mg^{2+} ions in the asymmetric unit. Biochemistry *41*, 9341–9348.
59. Hamy, F., Brondani, V., Florsheimer, A., Stark, W., Blommers, M.J.J., and Klimkait, T. (1998). A new class of HIV-1 Tat antagonist acting through Tat-TAR inhibition. Biochemistry *37*, 5086–5095.
60. White, S.A., and Draper, D.E. (1987). Single base bulges in small RNA hairpins enhance ethidium binding and promote an allosteric transition. Nucleic Acids Res. *15*, 4049–4064.
61. Li, H.J., and Crothers, D.M. (1969). Relaxation studies of the proflavine-DNA complex: the kinetics of an intercalation reaction. J. Mol. Biol. *39*, 461–477.
62. Mûller, W., Crothers, D.M., and Waring, M.J. (1973). A non-intercalating proflavine derivative. Eur. J. Biochem. *39*, 223–234.
63. Vagner, S., Galy, B., and Pyronnet, S. (2001). Irresistible IRES. EMBO *2*, 893–898.
64. Le, S.-Y., Siddiqui, A., and Maizel, J.V., Jr. (1996). A common structural core in the internal ribosome entry sites of picornavirus, hepatitis C virus, and pestivirus. Virus Genes *12*, 135–147.
65. Zell, R., Sidigi, K., Henke, A., Schmidt-Brauns, J., Hoey, E., Martin, S., and Stelzner, A. (1999). Functional features of the bovine enterovirus 5′-non-translated region. J. Gen. Virol. *80*, 2299–2309.
66. Siafakas, N., Markoulatos, P., and Stanway, G. (2002). Molecular classification of coxsackie A viruses on the basis of the 5′-UTR: structural and evolutionary aspects. J. Mol. Evol. *55*, 638–652.
67. Haldeman, R., Darós, J.-A., and Carrington, J.C. (1998). Secondary structures in the capsid protein coding sequence and 3′ nontranslated region involved in amplification of the tobacco etch virus genome. J. Virol. *72*, 4072–4079.
68. Proutski, V., Gould, E.A., and Holmes, E.C. (1997). Secondary structure of the 3′ untranslated region of flaviviruses: similarities and differences. Nucleic Acids Res. *25*, 1194–1202.
69. Atherton, E., and Sheppard, R.C. (1989). Solid-Phase Peptide Synthesis: A Practical Approach (Oxford: IRL Press).
70. Furka, Á., Sebestyén, F., Asgedom, M., and Dibó, G. (1991). General method for rapid synthesis of multicomponent peptide mixtures. Int. J. Pept. Protein Res. *37*, 487–493.
71. Sambrook, J., Fritsch, E.F., and Maniantis, T. (1989). Molecular Cloning: A Laboratory Manual, Second Edition (New York: Cold Spring Harbor Laboratory Press).